

Experimental quantum coding against qubit loss error

Chao-Yang Lu ^{*},¹ Wei-Bo Gao ^{*},¹ Jin Zhang,¹ Xiao-Qi Zhou,¹ Tao Yang,¹ and Jian-Wei Pan [§]^{1,2}

¹*Hefei National Laboratory for Physical Sciences at Microscale and Department of Modern Physics,
University of Science and Technology of China, Hefei, Anhui 230026, P. R. China*

²*Physikalisches Institut, Universität Heidelberg, Philosophenweg 12, 69120 Heidelberg, Germany*
(Dated: April 14, 2008)

A significant obstacle for practical quantum computation is the loss of physical qubits in quantum computers, a decoherence mechanism most notably in optical systems. Here we experimentally demonstrate, both in the quantum circuit model and in the one-way quantum computer model, the smallest non-trivial quantum codes to tackle this problem. In the experiment, we encode single-qubit input states into highly-entangled multiparticle codewords, and we test their ability to protect encoded quantum information from detected one-qubit loss error. Our results prove the in-principle feasibility of overcoming the qubit loss error by quantum codes.

Quantum computers are expected to harness the strange properties of quantum mechanics such as superposition and entanglement for enhanced ways of information processing. However, it has proved extremely difficult to build such devices in practice. Arguably the most formidable hurdle is the unavoidable decoherence caused by the coupling of the quantum computers to the environment which destroys the fragile quantum information rapidly. It is thus of crucial importance to find ways to reduce the decoherence and carry out coherent quantum operations in the presence of noise.

Recent experiments have made progresses toward this goal by demonstrating quantum error correction [1, 2, 3, 4, 5], decoherence-free subspace [6, 7, 8, 9] and entanglement purification [10, 11]. These experiments were designed to cope with one special kind of decoherence, that is, when qubits become entangled with the environment or undergo unknown rotations in the qubit space. Such errors can be represented as linear combinations of the standard errors: no error, bit-flip, phase-flip, or both.

There is, however, another significant source of error — the loss of qubits in quantum computers. The qubit, which is the basic element of standard quantum computation (QC), is supposed to be an isolated two-level system consisting of a pair of orthonormal quantum states. However, the majority of proposed quantum hardware are in fact multi-level systems, and the states of qubits are defined in a two-level subspace, which may leak out of the desired qubit space and into a larger Hilbert space [12, 13, 14]. This problem is common in practical QC with various qubits candidates, such as Josephson junctions [15], neutral atoms in optical lattices [16], and, most notoriously, single photons which can be lost during processing or owing to inefficient photon sources and detectors [17, 18, 19, 20, 21]. The loss of physical qubits is detrimental to QC since the working of quantum gates, algorithms and error correction codes (see e.g. [22, 23, 24]) all hinge on the percept that the quantum system remains in the qubit space.

Here we demonstrate the smallest meaningful quantum codes to protect quantum information from detected one-

qubit loss. Our experiment deals with qubit loss in both the quantum circuit model and one-way quantum computer model [25]. We encode single-qubit states into loss-tolerant codes which are multiparticle entangled states. The performances of the quantum codes are tested by determining the fidelities of the recovered states compared to the ideal original states. Our results verify that the qubit loss error could in principle be overcome by quantum codes.

Theoretical schemes

We now briefly review the quantum codes designed to tackle the problem of qubit loss. A special class of quantum erasure-error correction (QEEC) code was proposed by Grassl *et al.*, where a four-qubit code is sufficient to correct a detected one-qubit loss error [26]. The QEEC code was utilized by Knill *et al.* to deal with the photon-loss problem for scalable photonic QC [18]. In recent years, extensive efforts have been devoted to devising loss-tolerant quantum computer architectures [27, 28, 29, 30]. In particular, in the quantum circuit model Ralph *et al.* employed an incremental parity encoding method to achieve efficient linear optics QC, and showed a loss-tolerant optical memory was possible with a loss probability below 0.18 [29]. In the new approach known as the one-way QC, Varnava *et al.* exploited the inherent correlations in cluster states and introduced a novel scheme for fault-tolerantly coping with losses in the one-way QC that can tolerate up to 50% qubit loss [30].

QEEC codes

To show the principle of the QEEC codes [26], let us start with a specific example: a four-qubit code which is able to protect a logical qubit from loss of a physical qubit. Here a logical qubit $|\psi\rangle_l = a_0|0\rangle_l + a_1|1\rangle_l$ is encoded in the subspace with four physical qubits as

$$\begin{aligned} |0\rangle_l &= (|0\rangle_1|0\rangle_2 + |1\rangle_1|1\rangle_2)(|0\rangle_3|0\rangle_4 + |1\rangle_3|1\rangle_4) \\ |1\rangle_l &= (|0\rangle_1|0\rangle_2 - |1\rangle_1|1\rangle_2)(|0\rangle_3|0\rangle_4 - |1\rangle_3|1\rangle_4) \end{aligned} \quad (1)$$

This code can also be viewed as a combination of parity and redundant encoding, which is the basic module in Ralph's scheme of loss-tolerant optical QC [29].

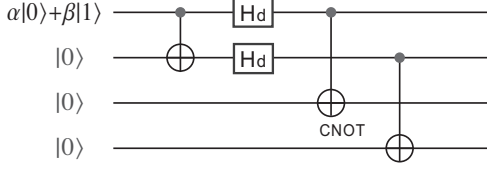


FIG. 1: A quantum circuit with two Hadamard (H_d) gates and three CNOT gates for implementation of the four-qubit QEEC code. The stabilizer generators of the QEEC code are $X \otimes X \otimes X \otimes X$ and $Z \otimes Z \otimes Z \otimes Z$, where X (Z) is short for Pauli matrix σ_x (σ_z) [24]. As proposed by Vaidman *et al.*, this four-qubit code can also be used for error detection [33].

We can consider the effect of a qubit loss as an unintended measurement from which we learn no information. The main feature of the code (1) is that the detected loss of any one of the physical qubits will not destroy the information of the logical qubit, but merely yields a recoverable Pauli error. Suppose for example, qubit 1 is lost. We first measure the qubit 2 in computational ($|0\rangle/|1\rangle$) basis. With its measurement result ($q_2 = 0$ or 1), we can obtain a pure quantum state $|\psi'\rangle_l = a_0(|0\rangle_3|0\rangle_4 + |1\rangle_3|1\rangle_4) + (-1)^{q_2}a_1(|0\rangle_3|0\rangle_4 - |1\rangle_3|1\rangle_4)$. With similar reasoning, more-qubit loss can also be corrected by increasing the size of loss-tolerant codes in the form of $|\Psi\rangle_l = a_0(|0\rangle^{\otimes n} + |1\rangle^{\otimes n})^{\otimes m} + b_0(|0\rangle^{\otimes n} - |1\rangle^{\otimes n})^{\otimes m}$, which can be created *e.g.*, by the incremental encoding scheme proposed in Ref. [29].

Demonstration of the QEEC code

A quantum circuit to implement the encoding of the four-qubit QEEC code is shown in Fig. 1. To implement this, we design a linear optics network (see Fig. 2A). The physical qubits are encoded by the polarizations of photons, with 0 corresponding to the horizontal (H) polarization and 1 to the vertical (V). As shown in ref. [31, 32], such an encoding method naturally incorporates a loss detection mechanism and may enable high-fidelity linear optical QC. Our experimental setup is illustrated in Fig. 2B. We use spontaneous parametric down conversion [34] to create the primary photonic qubits, which are then coherently manipulated by linear optical elements to implement the coding circuit and read out using single-photon detectors (see the caption of Fig. 2B and Methods).

To demonstrate the quantum codes work for general unknown states, we test three different input states: $|V\rangle$, $|+\rangle$, and $|R\rangle = (|H\rangle + i|V\rangle)/\sqrt{2}$, which are encoded into the four-qubit QEEC codes respectively as (normalizations omitted)

$$\begin{aligned} |V\rangle_l &= (|H\rangle_2|H\rangle_3 - |V\rangle_2|V\rangle_3)(|H\rangle_4|H\rangle_5 - |V\rangle_4|V\rangle_5), \\ |+\rangle_l &= (|H\rangle_2|H\rangle_3|H\rangle_4|H\rangle_5 + |V\rangle_2|V\rangle_3|V\rangle_4|V\rangle_5), \\ |R\rangle_l &= (|H\rangle_2|H\rangle_3 + |V\rangle_2|V\rangle_3)(|H\rangle_4|H\rangle_5 + |V\rangle_4|V\rangle_5) \\ &\quad + i(|H\rangle_2|H\rangle_3 - |V\rangle_2|V\rangle_3)(|H\rangle_4|H\rangle_5 - |V\rangle_4|V\rangle_5), \end{aligned}$$

where the subscript denotes the spatial mode. Inter-

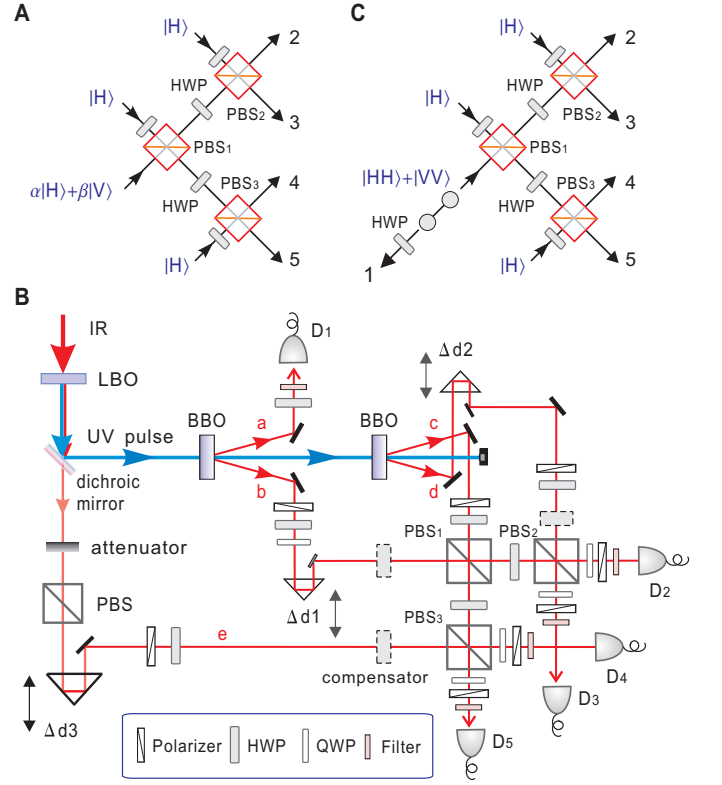


FIG. 2: The linear optical networks and experimental setup. **A.** We simulate the CNOT gate in Fig. 1 using a polarizing beam splitter (PBS) and a half-wave plate (HWP), through which a control photon ($\alpha|H\rangle + \beta|V\rangle$) and a target photon $|H\rangle$ evolve into $(\alpha|H\rangle|H\rangle + \beta|V\rangle|V\rangle)$ after postselection. Thus the circuit in Fig. 1 can be realized by this linear optical network. **B.** A pulsed infrared laser (788nm, 120fs, 76MHz) passes through a LiB_3O_5 (LBO) crystal where the laser is partially up-converted to ultraviolet ($\lambda=394\text{nm}$). Behind the LBO, five dichroic mirrors (only one shown) are used to separate the mixed ultraviolet (UV) and infrared light components. The reflected UV laser passes through two β -barium borate (BBO) crystals to produce two pairs of entangled photons. The transmitted infrared laser is further attenuated to a weak coherent photon source. To achieve good spatial and temporal overlap, the photons are spectrally filtered by narrow-band filters ($\Delta\lambda_{\text{FWHM}} = 3.2\text{nm}$, with peak transmission rates of $\sim 98\%$) and detected by fiber-coupled single-photon detectors (D_1, \dots, D_5) [37]. The compensator consists of a HWP sandwiched by two thin BBO crystals. By tilting the BBO, we can compensate the undesired phase shift in the PBS. **C.** The five-photon cluster state can be prepared by small modifications of the scheme of Fig. 2A.

estingly they show three distinct types of entanglement: $|V\rangle_l$ is a product state of two Einstein-Podolsky-Rosen (EPR) pairs [38], $|+\rangle_l$ is a four-qubit Greenberger-Horne-Zeilinger (GHZ) state [39], while $|R\rangle_l$ is locally equivalent to a cluster state [40].

We test the performance of the encoding process by determining fidelities of the encoded four-qubit states. The fidelities are judged by the overlap of the experimentally

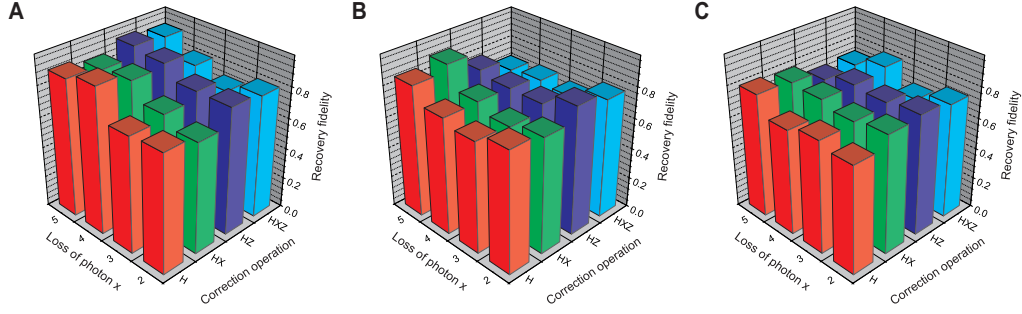


FIG. 3: Experimental results of recovering quantum information from detected qubit loss. Recovered state fidelities are listed for all possible cases of photon loss (2 or 3 or 4 or 5) and necessary feedforward correction operations (H_d or H_dX or H_dZ or H_dXZ). **A**, data for input state $|V\rangle$. **B**, for $|+\rangle$. **C**, for $|R\rangle$.

produced state with the ideal one: $F = \langle \psi | \rho_{\text{exp}} | \psi \rangle$. To do so, we first decompose $\rho = |\psi\rangle\langle\psi|$ into locally measurable observables which are products of Pauli operators [the detailed constructions are shown in the supporting information (SI) *Methods*]. For the states $|V\rangle_l$, $|+\rangle_l$ and $|R\rangle_l$ we need to take 9, 5 and 9 settings of four-photon polarization correlation measurements respectively, each composed of 2^4 coincidence detections to determine the probabilities of different outcome combinations. From the data shown in the SI *figures*, the fidelities of the QEEC codewords are: $F_V = 0.620 \pm 0.017$, $F_+ = 0.566 \pm 0.020$, $F_R = 0.554 \pm 0.017$. The fidelities of the four-qubit GHZ state and cluster state are above the threshold of 0.5, thus they are confirmed to contain genuine four-partite entanglement [41, 42]. The imperfections of the fidelities are caused mainly by high-order emissions of entangled photons and remaining distinguishability of independent photons overlapping on the PBSs. Finally, it should be noted that, as proposed in Ref. [2], for the purpose of “benchmarking” quantum computers, more settings of measurements will be needed to infer the average fidelity of the quantum coding.

“Loss-and-Recovery” test

Now we test the codes’ ability to protect the logical qubit information from one detected physical qubit loss through a “loss-and-recovery” process. Here we simulate the loss of a photon by detecting the photon without knowing its polarization information, which only tells us that the photon is lost. Experimentally, this is done by placing no polarizer or PBS in front of the detector.

In principle, the QEEC code works when only one and any one of the four physical qubits is lost. In our experiment, we test individually all possible cases where any single one of the four photons is lost. For instance, if we assume photon 2 is lost, the experimental procedure goes as follows. We erase the photon 2, perform a measurement in H/V basis on photon 3 and in $+/-$ basis on photon 4. Depending on different measurement results: $|H\rangle_3|+\rangle_4$, $|V\rangle_3|+\rangle_4$, $|H\rangle_3|-\rangle_4$, $|V\rangle_3|-\rangle_4$, correction operations: H_d , H_dX , H_dZ , H_dXZ should be applied on photon 5. As a proof-of-principle, here we apply correc-

tions for every individual outcome of photon 3 and 4, and determine the state fidelity of photon 5 compared to the original input state. For an explicit example, if we fix the polarizers in front of D_3 and D_4 in $|V\rangle$ and $|+\rangle$ polarization, we should apply H_dX to photon 5 and then measure its fidelity. Each measurement is flagged by a fivefold coincidence event where all five detectors fire simultaneously.

Figure 3 shows the measured recovery fidelities for all possible combinations. For input states $|V\rangle$, $|+\rangle$ and $|R\rangle$, the recovery fidelities averaged over all possible measurement outcomes are found to be 0.832 ± 0.012 , 0.764 ± 0.014 , and 0.745 ± 0.015 respectively, which well prove the effectiveness of the four-qubit QEEC codes. It can be noticed that the encoding and recovery fidelities for the state $|V\rangle$ is higher than those for $|+\rangle$ and $|R\rangle$. We believe this is because in our setup, the coding process for $|V\rangle$ requires interference of photons only on PBS_2 and PBS_3 whilst for the latter cases the interferences involve all three PBSs. Also it can be seen from Fig. 3A that for the input state $|V\rangle$, the recovery fidelities when we simulate photon 4 or 5 is lost are considerably better than those when photon 2 or 3 is lost. We note this is because in the former case, the interference involves with dependent photons c and d (from the same EPR pair) on the PBS_2 whilst the latter case requires interference of independent photons b and e on the PBS_3 .

Loss-tolerant one-way QC

Now we consider how to overcome the qubit loss in the one-way QC model [25]. In this model, QC is achieved by single-qubit measurements on prepared highly-entangled cluster states [40], where the orders and choices of measurements determine the algorithm computed. It is important to note that the loss-detection is naturally incorporated in the measurement step in this QC model.

To tackle fault tolerance in this architecture, novel protocols have been developed by exploiting the built-in properties of the entangled cluster states which provide natural resilience to decoherence [30, 45]. In particular, Varnava *et al.* utilized the tree-shaped graph states and analyzed that a high error threshold of 0.5 exists for qubit

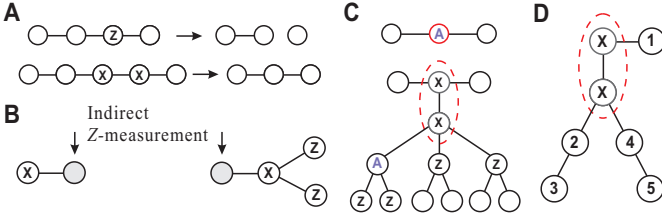


FIG. 4: Principle of the loss-tolerant one-way quantum computation scheme [30]. A cluster state can be represented by a graph, where the vertices take the role of qubits while the edges represent interaction [46]. **A.** Certain measurements on a cluster state have interesting effects: A Z measurement removes the qubit from the cluster and breaks all the bonds between the qubit and the rest; Two adjacent X measurements on a linear cluster remove the qubit and form direct bonds between their neighbors. **B.** A cluster state is an eigenstate of a set of stabilizers, which predict with certainty correlations in the measurement outcomes of certain sets of measurements. For instance, for a two-qubit state that is stabilized by the operator $X_1 Z_2$, if observable X_1 is measured then the outcome of Z_2 is known with certainty. This allows us to measure a qubit even if it is lost, which is called “indirect measurement” [30]. **C.** The tree-graph cluster state which can be used for reduction of the effective qubit loss rate. We plant a cluster tree by two adjacent X measurements, on which instead of doing the A measurement on the in-line qubit, we can perform the measurement on a qubit in the third horizontal level. When this measurement succeeds, we break the bounds with all other qubits in the tree. If it fails, we remove this damaged qubit and attempt the A measurement on other qubits in the third level. The tree structure ensures that the removal of damaged qubits can be done by direct or indirect Z measurements. **D.** The five-qubit cluster state can be used for an in-principle verification of this scheme.

loss error [30]. The salient feature of this scheme is illustrated in Fig. 4. Briefly, the tree graph state takes advantage of the perfect correlations in the cluster states and embodies two useful features that enable reduction of the effective qubit loss rate. First, it allows multiple attempts to do the desired measurement on an encoded qubit. Second, it is designed such that any given qubit within the cluster could be removed (see the caption of Fig. 4).

Creation of a five-qubit cluster state

We use a five-qubit cluster state for demonstration of Varnava *et al.*’s scheme [30]. As shown in Fig. 4D, it can be thought of as being reduced from a seven-qubit cluster after two adjacent X measurements. Alternatively, the cluster can be grown directly, as we do in our experiment.

Starting from an EPR pair and three single photons, we use the linear optical network shown in Fig. 2C and the experimental setup shown in Fig. 2B to create the five-photon cluster state (see Methods). When each of the five output modes registers a photon, the five photons

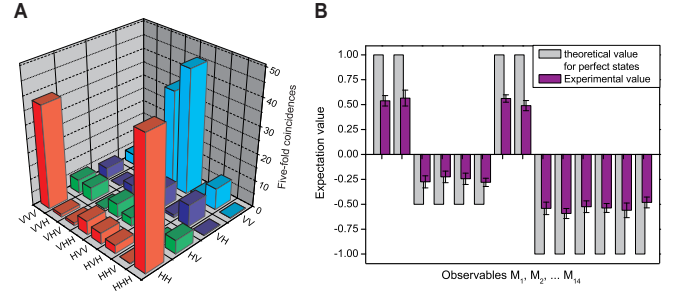


FIG. 5: Experimental results of the five-photon cluster state $|\phi_5\rangle$. **A.** Five-photon detection events in the H/V basis. **B.** Measured expectation values of the other 14 observables M_1, M_2, \dots, M_{14} (detailed representations shown in SI Methods) to determine the fidelity of the cluster state $|\phi_5\rangle$. The error bars denote one standard deviation, deduced from propagated Poissonian counting statistics of the raw detection events.

are in the highly-entangled cluster state

$$|\phi_5\rangle = \frac{1}{2} (|H\rangle_1 |H\rangle_2 |H\rangle_3 |H\rangle_4 |H\rangle_5 + |H\rangle_1 |V\rangle_2 |V\rangle_3 |V\rangle_4 |V\rangle_5 \\ + |V\rangle_1 |H\rangle_2 |H\rangle_3 |V\rangle_4 |V\rangle_5 + |V\rangle_1 |V\rangle_2 |V\rangle_3 |H\rangle_4 |H\rangle_5),$$

where the subscript labels the photon’s spatial mode (see Fig. 2C). The state $|\phi_5\rangle$ is local unitarily equivalent to the five-qubit linear cluster state shown in Fig. 4D under the H_d transformations on photon 1, 3 and 5. This is, to our best knowledge, the longest one-dimensional cluster state realized so far.

To determine the fidelity of the five-photon cluster state, we decompose the projector $|\phi_5\rangle\langle\phi_5|$ into 15 local measurable observables (see the SI Methods), each takes 2^5 five-fold coincidence measurements. The experimental results are shown in Fig. 5, yielding $F_c = \langle\phi_5|\rho_{exp}|\phi_5\rangle = 0.564 \pm 0.015$. As the fidelity of the cluster state exceeds 0.5, the presence of true five-partite entanglement of our cluster state is also confirmed [42].

One-way QC in the presence of loss

With the cluster state prepared, now we demonstrate its loss-tolerant feature by simulation of a quantum circuit in the presence of loss. First let us briefly review how QC is done by measurements in the one-way model. The measurement is chosen in basis $B_j(\alpha) = \{|+\alpha\rangle_j, |-\alpha\rangle_j\}$, where $|\pm\alpha\rangle_j = (|0\rangle_j \pm e^{i\alpha}|1\rangle_j)/\sqrt{2}$, which realizes the single-qubit rotation $R_z(\alpha) = \exp(-i\alpha\sigma_z/2)$ followed by a Hadamard operation on the encoded qubit in the cluster. We define the outcome $s_j = 0$ if the measurement on the physical qubit j yields $|+\alpha\rangle_j$, and $s_j = 1$ if it is $|-\alpha\rangle_j$. When $s_j = 0$, the computation proceeds without error, whereas when $s_j = 1$, a known Pauli error is introduced that has to be compensated for (see ref. [25, 43, 44] for more details).

The two-qubit cluster shown in Fig. 6A can implement a simple circuit, rotating an encoded input qubit $|+\rangle$ to an output state: $|\psi_{out}\rangle = X^{s_a} H_d R_z(\alpha) |+\rangle$. With this two-qubit cluster, however, one can only have a one-shot

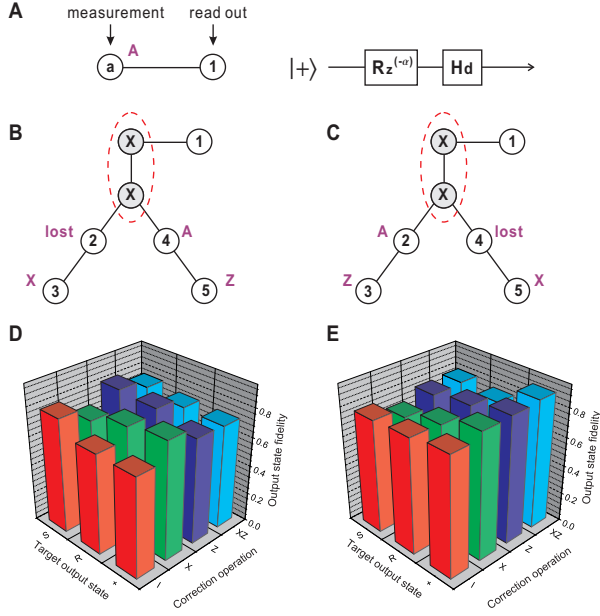


FIG. 6: Experimental results of loss-tolerant one-way quantum computing. **A.** A two-qubit cluster state used to simulate a single-qubit rotation circuit by a measurement on qubit a . **B-C.** A five-qubit cluster state could realize the circuit in the presence of one-qubit loss. **D-E.** The experimentally measured fidelities of output states of the single-qubit rotation circuit. **D** (**E**) shows the results of the scheme **B** (**C**) respectively. Measurements on the qubit 4 (2) are performed in basis $B_j(\alpha)$ for different α value, $\{0, -\pi/2, -\pi/3\}$ so that the target output state will be $\{|+\rangle, |R\rangle, |S\rangle\}$ respectively.

A measurement on the qubit a , that is, if this measurement fails then the whole computation fails. As a comparison, the five-qubit cluster state we prepared can be used to realize the circuit in a more robust fashion. It provides two alternative and equivalent attempts to do the A measurement as depicted in Fig. 6B and 6C. And if any one of the qubits (2, 3, 4, 5) for the A measurement is lost, we can always find a suitable indirect Z measurement to remove the damaged qubit. For example, if the A measurement on qubit 2 fails, we can try to remove it from the cluster by an indirect Z measurement, and then proceed to make the A measurement on qubit 4. It can be checked that as long as no more than one physical qubit is lost, the computation will be successful.

Now we demonstrate it experimentally. To verify the scheme depicted in Fig. 6B, we erase photon 2, which makes the remaining cluster in a mixed state. Then we make a X measurement (which corresponds to the H/V basis in the laboratory basis for the actual state $|\phi_5\rangle$) on photon 3 — this should effectively remove the loss error out of the cluster, leaving it as a smaller but pure quantum cluster state. Next the redundant photon 5 is measured in the Z basis (which corresponds to the laboratory basis $+/ -$). Depending on the measurement outcomes of photon 3 and 5 ($|H\rangle_3|+\rangle_5$, $|V\rangle_3|+\rangle_5$, $|H\rangle_3|-\rangle_5$,

$|V\rangle_3|-\rangle_5$), Pauli corrections (I, X, Z, XZ) are applied to photon 4. After that, measurements in the basis $B_j(\alpha)$ are applied on photon 4 to implement the rotation. We choose α to be three different values, $0, -\pi/2, -\pi/3$ so that theoretically the output states will be $|+\rangle$, $|R\rangle$ and $|S\rangle = (|0\rangle + e^{i\pi/3}|1\rangle)/\sqrt{2}$, respectively. Then we readout the polarizations of photon 1 and determine its fidelities compared to the ideal states. The scheme of Fig. 6C is also tested in a similar manner.

In Fig. 6D, 6E we show the experimental results of one-way QC in the presence of one-qubit loss. In the case of photon 2 lost, we find an average fidelity of 0.738 ± 0.029 , 0.750 ± 0.030 , and 0.765 ± 0.028 for target output state $|+\rangle$, $|R\rangle$ and $|S\rangle$ respectively. In the case of photon 4 lost, the average fidelity is 0.865 ± 0.021 , 0.792 ± 0.029 , and 0.767 ± 0.030 for target output state $|+\rangle$, $|R\rangle$ and $|S\rangle$. Here the difference of the fidelity performance is caused by similar reasons as in the QEEC codes. For instance, the case for target output state $|+\rangle$ corresponds to Fig. 3A where the input state is in the state of $|V\rangle$. These results conclusively demonstrate the underlying principle of loss-tolerant one-way QC.

Discussion

As in all current linear optical QC experiments, the multiphoton code states here are created probabilistically and conditioned on that there is one and only one photon out of each output, a technique called post-selection [37]. While this does not prevent an in-principle verification of the loss-tolerant quantum codes, we note eventual scalable implementations will need significant improvements such as on-demand entangled photon sources and high-efficiency single-photon detectors.

In summary, we have demonstrated both in the quantum circuit model and in the one-way model, the smallest meaningful quantum codes to protect quantum information from qubit loss error. These quantum codes are the key modules for the loss-tolerant quantum computer architectures [29, 30] and can in principle be extended to larger number of qubits. Our results verify that it is possible to overcome the qubit loss error, a major decoherence mechanism common in many physical systems, and thus constitute a necessary step toward scalable quantum information processing, especially for photon-based QC. The loss-tolerant quantum codes can be further concatenated with standard quantum error correction codes [22, 23, 24] or decoherence free space [6, 7, 8, 9] to correct multiple errors, and may become a useful part for future implementations of quantum algorithms [43, 44, 47, 48, 49, 50].

Methods

Experimental implementation We first prepare two entangled photon pairs in spatial modes $a-b$ and $c-d$ with an average coincidence count of $\sim 6.2 \times 10^4 s^{-1}$, and a pseudo-single photon source in mode e , which has a very small probability (p) of containing a single photon for each pulse. The p value is carefully chosen to be ~ 0.07

experimentally to get an optimal visibility [35]. Photon a serves as a trigger, indicating that the pair photon b is under way; Photon b is prepared in different input states; Photon c, d, e are initialized in the $+45^\circ$ linear polarization state $|+\rangle = (|H\rangle + |V\rangle)/\sqrt{2}$. We superpose photon b, c, d, e on the three PBSs step by step. For alignment on the PBS₁, for instance, we first initialize the two photons b and c at state $|+\rangle$ before they enter into the PBS₁, and, by making fine adjustment of delay Δd_1 , we are able to observe the two-photon Hong-Ou-Mandel type dip [36] after the PBS₁ by performing polarization measurements in both output modes in the $|\pm\rangle = (|H\rangle \pm |V\rangle)/\sqrt{2}$ basis. Similarly, optimal superpositions of the photons on the other two PBSs are also achieved. The optimal interference occurs at the regime of zero delay, where our experimental measurements are performed. Note some PBSs may have undesired phase shifts, that is, when two input photons that prepared in the states of $|+\rangle$ are superposed on the PBSs, the output photons are not in the expected state of $(|H\rangle|H\rangle + |V\rangle|V\rangle)/\sqrt{2}$ but in the state of $(|H\rangle|H\rangle + e^{i\theta}|V\rangle|V\rangle)/\sqrt{2}$ with a θ phase shift. This can be overcome by a compensator (see Fig. 2B) which can introduce a phase delay between $|H\rangle$ and $|V\rangle$.

Five-photon cluster state preparation An EPR photon pair is prepared in the spatial mode a - b in the state $(|H\rangle_a|H\rangle_b + |V\rangle_a|V\rangle_b)/\sqrt{2}$ with a visibility of 92% in the $+/-$ basis. We note that this non-perfect visibility may add additional noise into the five-photon cluster state compared to the four-photon states using the scheme as shown in Fig. 2A. To get a better fidelity for the cluster state, we lower the pump power and obtain an average coincidence of $\sim 5.0 \times 10^4 s^{-1}$ in modes a - b and c - d , such that the rate of double pair emission of entangled photons is diminished. Meanwhile, the p value for the pseudo-single photon source is also reduced to ~ 0.06 accordingly.

Acknowledgements: We thank T. Rudolph, D. Browne, O. Gühne, T. Ralph and M. Zukowski for helpful discussions. This work was supported by the NNSF of China, the CAS and the National Fundamental Research Program (under Grant No. 2006CB921900). This work was also supported by the Alexander von Humboldt Foundation and Marie Curie Excellence Grant of the EU.

The authors declare no conflict of interest.

* These authors contributed equally to this work.

§ Correspondence and request for materials should be sent to C.-Y.L (cylu@mail.ustc.edu.cn) and J.-W.P (jianwei.pan@physi.uni-heidelberg.de).

-
- [1] Cory, D. G. *et al.* Experimental quantum error correction. *Phys. Rev. Lett.* **81**, 2152-2155 (1998).
 [2] Knill, E., Laflamme, R., Martinez, R., Negrevergne, C. Benchmarking quantum computers: The five-qubit error correcting code. *Phys. Rev. Lett.* **86**, 5811-5814 (2001).

- [3] Chiaverini, J., *et al.* Realization of quantum error correction. *Nature* **432**, 602-605 (2004).
 [4] Pittman, T.B., Jacobs, B.C., and Franson, J.D., Demonstration of quantum error correction using linear optics. *Phys. Rev. A* **71**, 052332 (2005).
 [5] O'Brien, J.L., Pryde, G.J., White, A.G., and Ralph, T.C. High-fidelity Z-measurement error encoding of optical qubits. *Phys. Rev. A* **71**, 060303 (2005).
 [6] Kwiat, P.G., Berglund, A.J., Altepeter, J.B., White, A.G., Experimental verification of decoherence-free subspaces. *Science* **290**, 498-501 (2000).
 [7] Kielpinski, D. *et al.*, A decoherence-free quantum memory using trapped ions. *Science* **291**, 1013-1015 (2000).
 [8] Bourennane, M. *et al.*, Decoherence-free quantum information processing with four-photon entangled states. *Phys. Rev. Lett.* **92**, 107901 (2003).
 [9] Prevedel, R. *et al.*, Experimental demonstration of decoherence-free one-way information transfer. *Phys. Rev. Lett.* **99**, 250503 (2007).
 [10] Pan, J.-W. *et al.* Experimental entanglement purification of arbitrary unknown states. *Nature* **423**, 417-422 (2003).
 [11] Reichle, R. Experimental purification of two-atom entanglement. *Nature* **443**, 838-841 (2006).
 [12] Preskill, J. Reliable quantum computers. *Proc. R. Soc. Lond. A* **454**, 385-410 (1998).
 [13] Wu, L.-A., Byrd, M.S., and Lidar, D.A. Efficient Universal Leakage Elimination for Physical and Encoded Qubits. *Phys. Rev. Lett.* **89**, 127901 (2002).
 [14] Devitt, S.J., *et al.* Subspace confinement: how good is your qubit? *New J. Phys.* **9** 384 (2007).
 [15] Fazio, R., Palma, G.M., Siewert, J., Fidelity and leakage of Josephson qubits. *Phys. Rev. Lett.* **83**, 5385-5388 (1999).
 [16] Vala, J., Whaley, K.B., Weiss, D.S., Quantum error correction of a qubit loss in an addressable atomic system. *Phys. Rev. A* **72**, 052318 (2005).
 [17] Kok, P., *et al.* Linear optical quantum computing with photonic qubits. *Rev. Mod. Phys.* **79**, 135 (2007).
 [18] Knill, E., Laflamme, R., Milburn, G. J. A scheme for efficient quantum computation with linear optics. *Nature* **409**, 46-52 (2001).
 [19] Knill, E., Scalable quantum computing in the presence of large detected-error rates. *Phys. Rev. A* **71**, 042322 (2005).
 [20] Silva, M., Rötteler, M., Zalka, C., Thresholds for linear optics quantum computing with photon loss at the detectors. *Phys. Rev. A* **72**, 032307 (2005).
 [21] Wasilewski, W., and Banaszek, K., Protecting an optical qubit against photon loss. *Phys. Rev. A* **75**, 042316 (2007).
 [22] Calderbank, A. R., Shor, P. W. Good quantum error-correcting codes exist. *Phys. Rev. A* **54**, 1098-1105 (1996).
 [23] Steane, A. M. Error correcting codes in quantum theory. *Phys. Rev. Lett.* **77**, 793-797 (1996).
 [24] Gottesman, D., Stabilizer codes and quantum error correction. Ph.D. thesis, California Institute of Technology (1997).
 [25] Raussendorf, R., Briegel, H. J. A one-way quantum computer. *Phys. Rev. Lett.* **86**, 5188-5191 (2001).
 [26] Grassl, M., Beth, T., Pellizari, T. Codes for the quantum erasure channel. *Phys. Rev. A* **56**, 33-38 (1997).
 [27] Aliferis, P., Terhal, B.M., Fault-tolerant quantum computation for local leakage faults. *Quant. Inf. Comp.* **7**,

- 139-156 (2007).
- [28] Knill, E., Quantum computing with realistically noisy devices. *Nature* **434**, 39-44 (2005).
 - [29] Ralph, T.C., Hayes, A.J.F., Gilchrist, A., Loss-tolerant optical qubits. *Phys. Rev. Lett.* **95**, 100501 (2005).
 - [30] Varnava, M., Browne, D. E., Rudolph, T. Loss tolerance in one-way quantum computation via counterfactual error correction. *Phys. Rev. Lett.* **97**, 120501 (2006).
 - [31] Spedalieri, F.M., Lee, H., and Dowling, J.P., High-fidelity linear optical quantum computing with polarization encoding. *Phys. Rev. A* **73**, 012334 (2006).
 - [32] Gilchrist, A., Hayes, A.J.F., Ralph, T.C., Efficient parity-encoded optical quantum computing. *Phys. Rev. A* **75**, 052328 (2007).
 - [33] Vaidman, L., Goldenberg, L., and Wiesner, S. Error prevention scheme with four particles. *Phys. Rev. A* **54**, 1745-1748 (1996).
 - [34] Kwiat, P. G. *et al.* New high intensity source of polarization-entangled photon pairs. *Phys. Rev. Lett.* **75**, 4337-4341 (1995).
 - [35] Rarity, J. G. Tapster, P. R. Three-particle entanglement from entangled photon pairs and a weak coherent state. *Phys. Rev. A* **59**, R35-R38 (1999).
 - [36] Hong, C. K., Ou, Z. Y., Mandel, L. Measurement of sub-picosecond time intervals between two photons by interference. *Phys. Rev. Lett.* **59**, 2044-2046 (1987).
 - [37] Bouwmeester, D., *et al.* Experimental quantum teleportation. *Nature* **390**, 575-579 (1997).
 - [38] Einstein, A., Podolsky, B., Rosen, N. Can quantum-mechanical description of physical reality be considered complete? *Phys. Rev.* **47**, 777-780 (1935).
 - [39] Greenberger, D. M., Horne, M. A., Shimony, A., Zeilinger, A. Bell's theorem without inequalities. *Am. J. Phys.* **58**, 1131-1143 (1990).
 - [40] Briegel, H. J., Raussendorf, R. Persistent entanglement in arrays of interacting particles. *Phys. Rev. Lett.* **86**, 910-913 (2001).
 - [41] Bourennane, M. *et al.* Experimental detection of multipartite entanglement using witness operators. *Phys. Rev. Lett.* **92**, 087902 (2004).
 - [42] Toth, G., Gühne, O. Entanglement detection in the stabilizer formalism. *Phys. Rev. A* **72**, 022340 (2005).
 - [43] Walther, P. *et al.* Experimental one-way quantum computing. *Nature* **434**, 169-176 (2005).
 - [44] Prevedel, R., *et al.* High-speed linear optics quantum computation using active feed-forward. *Nature* **445**, 65-69 (2007).
 - [45] Raussendorf, R., Harrington, J., Goyal, K., Topological fault-tolerance in cluster state quantum computation. *New J. Phys.* **9**, 199 (2007).
 - [46] Hein, M., Eisert, J., Briegel, H.-J. Multiparty entanglement in graph states. *Phys. Rev. A* **69**, 062311 (2004).
 - [47] Vandersypen, L.M.K., *et al.* Experimental realization of Shor's quantum factoring algorithm using nuclear magnetic resonance. *Nature* **414**, 883-887 (2001).
 - [48] Kwiat, P.G., *et al.* Grover's search algorithm: an optical approach. *J. Mod. Opt.* **47**, 257 (2000).
 - [49] Lu, C.-Y. *et al.* Demonstration of a compiled version of Shor's quantum factoring algorithm using photonic qubits. *Phys. Rev. Lett.* **99**, 250504 (2007).
 - [50] Lanyon, B.P., *et al.* Experimental demonstration of a compiled version of Shor's algorithm with quantum entanglement. *Phys. Rev. Lett.* **99**, 250505 (2007).

Experimental quantum coding against qubit loss error: supporting information

Chao-Yang Lu ^{*},¹ Wei-Bo Gao ^{*},¹ Jin Zhang,¹ Xiao-Qi Zhou,¹ Tao Yang,¹ and Jian-Wei Pan [§]^{1,2}

¹*Hefei National Laboratory for Physical Sciences at Microscale and Department of Modern Physics,
University of Science and Technology of China, Hefei, Anhui 230026, P. R. China*

²*Physikalisches Institut, Universität Heidelberg,
Philosophenweg 12, 69120 Heidelberg, Germany*

(Dated: March 31, 2008)

Methods

The determination of the state fidelity and the detection of entanglement are fundamental problems in quantum information. This task is usually difficult in experiments especially for systems with many particles. Instead of using quantum state tomography [1] which would require about 4^N (N is the number of qubits) measurements, in our experiment, we use a method similar to entanglement witness [2, 3] which requires only a linear experimental effort.

In an experiment, one typically aims at the creation of some pure entangled multi-qubit state $|\Phi\rangle$. The fidelity of the produced state, that is, to what extent the desired state was prepared, is given by $F = \langle \Phi | \rho_{\text{exp}} | \Phi \rangle$ and should ideally equal to one. For experimental implementations, it is necessary to decompose $|\Phi\rangle\langle\Phi|$ into a number of local von Neumann (or projective) measurements [4]. The detailed constructions of the states $|V\rangle_l, |+\rangle_l, |R\rangle_l, |\Phi_5\rangle$ are as follows.

(1) The four-photon QEEC codeword of $|V\rangle$ is

$$|V\rangle_l = \frac{1}{2}(|H\rangle_2|H\rangle_3 - |V\rangle_2|V\rangle_3)(|H\rangle_4|H\rangle_5 - |V\rangle_4|V\rangle_5).$$

We can decompose $|V\rangle_l$ into locally measurable observables

$$|V\rangle_l\langle V| = \frac{1}{16}(I + Z_2Z_3 - X_2X_3 - Y_2Y_3)(I + Z_4Z_5 - X_4X_5 - Y_4Y_5),$$

where I denotes the identity operator, and Z, X, Y are short for the Pauli matrix $\sigma_z, \sigma_x, \sigma_y$ respectively. To determine the expectation value of $|V\rangle_l\langle V|$, we need to take 9 measurement settings, namely $X_2X_3X_4X_5, X_2X_3Y_4Y_5, X_2X_3Z_4Z_5, Y_2Y_3X_4X_5, Y_2Y_3Y_4Y_5, Y_2Y_3Z_4Z_5, Z_2Z_3X_4X_5, Z_2Z_3Y_4Y_5, Z_2Z_3Z_4Z_5$. Here, as used in literatures [2–4], a measurement setting refers to that can be measured at the same time without changing the experimental setup.

Let us take the measurement setting $X_2X_3Z_4Z_5$ as an example to show how the expectation values of observables $X_2X_3Z_4Z_5$, $X_2X_3I_4I_5$ and $I_2I_3Z_4Z_5$ are derived from the experimental data. The spin observable Z corresponds to a measurement of the H/V linear polarization, and X (Y) corresponds to the analysis of $\pm 45^\circ$ linear polarization (left/right circular polarization). For polarization analysis, half and quarter-wave plates (HWP, QWP) together with polarizers or PBSs are used. We use a programmable multichannel coincidence unit to register the five-fold coincidence events. Here for the measurement of the four-photon QEEC codes, the signal of detector 1 (D_1) is used only as a trigger. In this setting $X_2X_3Z_4Z_5$, we register the five-fold coincidence counts of the 16 different polarization combinations ($|+\rangle_2|+\rangle_3|H\rangle_4|H\rangle_5$, $|+\rangle_2|+\rangle_3|H\rangle_4|V\rangle_5$, $|+\rangle_2|+\rangle_3|V\rangle_4|H\rangle_5$, \dots $|-\rangle_2|-\rangle_3|V\rangle_4|V\rangle_5$), each signaling the observation of an eigenstate of the observable $X_2X_3Z_4Z_5$ (also $X_2X_3I_4I_5$ and $I_2I_3Z_4Z_5$) with the corresponding eigenvalue of $v_j = +1$ or $v_j = -1$. From the probabilities of multiphoton detections p_j , $j = 1, 2, \dots, 16$, we can then compute the expectation values of the observables by $\sum_{j=1}^{16} p_j v_j$. The full experimental results for the state $|V\rangle_l$ is shown in SI figure 1.

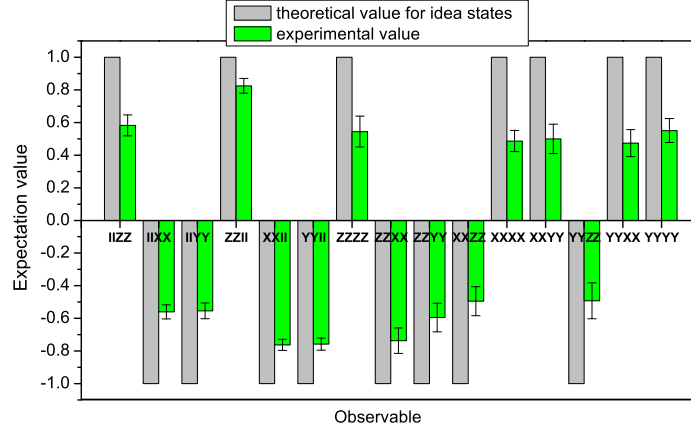


FIG. 1: Experimental result of the four-photon QEEC code $|V\rangle_l$. Expectation values of the 15 observables ($IIZZ$, $IIXX$, $YYYY$) are listed. Each of them is derived from a complete set of 16 five-fold coincidence events. The error bars denote one-standard deviations, deduced from propagated Poissonian counting statistics of the raw detection events.

(2) The encoded state of $|+\rangle = \frac{1}{\sqrt{2}}(|H\rangle + |V\rangle)$ is

$$|+\rangle_l = \frac{1}{\sqrt{2}}(|H\rangle_2|H\rangle_3|H\rangle_4|H\rangle_5 + |V\rangle_2|V\rangle_3|V\rangle_4|V\rangle_5).$$

The decomposition of $|+\rangle_l$ is:

$$|+\rangle_l \langle +| = \frac{1}{2}(|HHHH\rangle_{2345} \langle HHHH| + |VVVV\rangle_{2345} \langle VVVV|) + \frac{1}{8}(X_2 X_3 X_4 X_5 + Y_2 Y_3 Y_4 Y_5 - (\frac{X+Y}{\sqrt{2}})^{\otimes 4} - (\frac{X-Y}{\sqrt{2}})^{\otimes 4})$$

Here we need to take 5 measurement settings, namely $Z_2 Z_3 Z_4 Z_5$, $X_2 X_3 X_4 X_5$, $Y_2 Y_3 Y_4 Y_5$, $(\frac{X+Y}{\sqrt{2}})^{\otimes 4}$, and $(\frac{X-Y}{\sqrt{2}})^{\otimes 4}$. $(|HHHH\rangle_{2345} \langle HHHH| + |VVVV\rangle_{2345} \langle VVVV|)$ can be calculated as the population of the sum of $HHHH$ and $VVVV$ events. The spin operator $(X+Y)/\sqrt{2}$ $((X-Y)/\sqrt{2})$ corresponds to a measurement in the polarization basis $(H \pm e^{i\pi/4}V)/\sqrt{2}$ $((H \pm e^{-i\pi/4}V)/\sqrt{2})$. The experimental results for the state $|+\rangle_l$ is shown in SI figure 2.

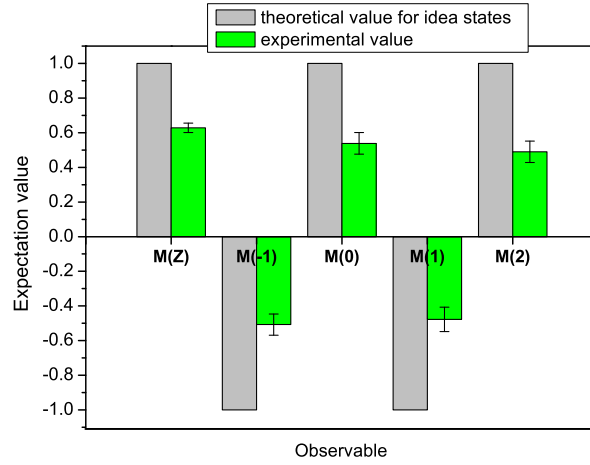


FIG. 2: Experimental result of the four-photon QEEC code $|+\rangle_l$. Here $M(Z) = (|HHHH\rangle \langle HHHH| + |VVVV\rangle \langle VVVV|)$, $M(-1) = (\frac{X-Y}{\sqrt{2}})^{\otimes 4}$, $M(0) = X_2 X_3 X_4 X_5$, $M(1) = (\frac{X+Y}{\sqrt{2}})^{\otimes 4}$, $M(-2) = Y_2 Y_3 Y_4 Y_5$.

(3) The encoded state of $|R\rangle = \frac{1}{\sqrt{2}}(|H\rangle + i|V\rangle)$ is

$$|R\rangle_l = \frac{1}{2\sqrt{2}}[(|H\rangle_2 |H\rangle_3 + |V\rangle_2 |V\rangle_3)(|H\rangle_4 |H\rangle_5 + |V\rangle_4 |V\rangle_5) + i(|H\rangle_2 |H\rangle_3 - |V\rangle_2 |V\rangle_3)(|H\rangle_4 |H\rangle_5 - |V\rangle_4 |V\rangle_5)]$$

The decomposition of $|R\rangle$ is:

$$|R\rangle_l \langle R| = \frac{1}{4}[(|HHHH\rangle \langle HHHH| + |VVVV\rangle \langle VVVV| + |HHVV\rangle \langle HHVV| + |VVHH\rangle \langle VVHH|)] + \frac{1}{16}(X_2 X_3 X_4 X_5 + Y_2 Y_3 Y_4 Y_5 - X_2 X_3 Y_4 Y_5 - Y_2 Y_3 X_4 X_5) - \frac{1}{16}[(Z_2 + Z_3)(Y_4 X_5 + X_4 Y_5) + (Y_2 X_3 + X_2 Y_3)(Z_4 + Z_5)]$$

The experimental results for the state $|R\rangle_l$ is shown in SI figure 3.

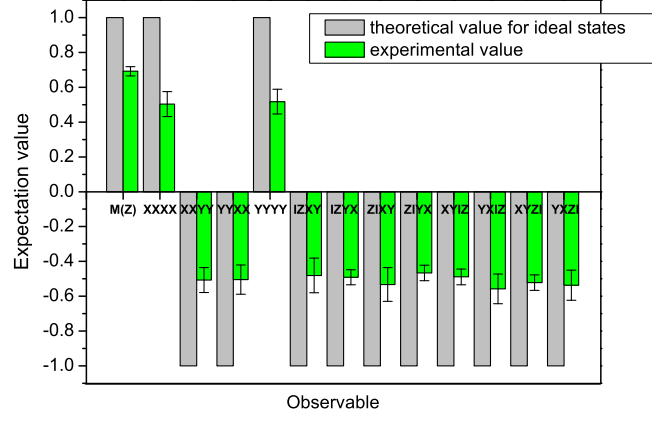


FIG. 3: Experimental result of the four-photon QEEC code $|R\rangle_l$. Here $M(Z) = (|HHHH\rangle\langle HHHH| + |VVVV\rangle\langle VVVV| + |HHVV\rangle\langle HHVV| + |VVHH\rangle\langle VVHH|)$.

(4) The five-photon cluster state can be written as

$$|\Phi_5\rangle = \frac{1}{2} [|H\rangle_1 (|HHHH\rangle_{2345} + |VVVV\rangle_{2345}) + |V\rangle_1 (|HHVV\rangle_{2345} + |VVHH\rangle_{2345})]$$

The decomposition of $|\Phi_5\rangle$ is:

$$\begin{aligned} |\Phi_5\rangle\langle\Phi_5| = & \frac{1}{4} (|HHHHH\rangle\langle HHHHH| + |HVVVV\rangle\langle HVVVV| \\ & + |VHHVV\rangle\langle VHHVV| + |VVVHH\rangle\langle VVVHH|) \\ & + \frac{1}{16} [I_1 X_2 X_3 X_4 X_5 + I_1 Y_2 Y_3 Y_4 Y_5 - |H\rangle_1 \langle H| \left(\frac{X+Y}{\sqrt{2}}\right)^{\otimes 4} - |H\rangle_1 \langle H| \left(\frac{X-Y}{\sqrt{2}}\right)^{\otimes 4} \\ & - |V\rangle_1 \langle V| \left(\frac{X+Y}{\sqrt{2}}\right)^{\otimes 2} \left(\frac{X-Y}{\sqrt{2}}\right)^{\otimes 2} - |V\rangle_1 \langle V| \left(\frac{X-Y}{\sqrt{2}}\right)^{\otimes 2} \left(\frac{X+Y}{\sqrt{2}}\right)^{\otimes 2} \\ & + (|HH\rangle_{23} \langle HH| + |VV\rangle_{23} \langle VV|) X_1 X_4 X_5 - (|HH\rangle_{23} \langle HH| + |VV\rangle_{23} \langle VV|) X_1 Y_4 Y_5 \\ & + X_1 X_2 X_3 (|HH\rangle_{45} \langle HH| + |VV\rangle_{45} \langle VV|) - X_1 Y_2 Y_3 (|HH\rangle_{45} \langle HH| + |VV\rangle_{45} \langle VV|) \\ & - (|HH\rangle_{23} \langle HH| - |VV\rangle_{23} \langle VV|) Y_1 X_4 Y_5 - (|HH\rangle_{23} \langle HH| - |VV\rangle_{23} \langle VV|) Y_1 Y_4 X_5 \\ & - Y_1 X_2 Y_3 (|HH\rangle_{45} \langle HH| - |VV\rangle_{45} \langle VV|) - Y_1 Y_2 X_3 (|HH\rangle_{45} \langle HH| - |VV\rangle_{45} \langle VV|)] \end{aligned}$$

The observables (M_1, M_2, \dots, M_{14}) listed in main text Figure 5B are as follows:

$$\begin{aligned}
M_1 &= I_1 X_2 X_3 X_4 X_5, \\
M_2 &= I_1 Y_2 Y_3 Y_4 Y_5, \\
M_3 &= |H\rangle_1 \langle H| \left(\frac{X+Y}{\sqrt{2}} \right)_{23}^{\otimes 4}, \\
M_4 &= |H\rangle_1 \langle H| \left(\frac{X-Y}{\sqrt{2}} \right)_{23}^{\otimes 4}, \\
M_5 &= |V\rangle_1 \langle V| \left(\frac{X+Y}{\sqrt{2}} \right)_{23}^{\otimes 2} \left(\frac{X-Y}{\sqrt{2}} \right)_{45}^{\otimes 2}, \\
M_6 &= |V\rangle_1 \langle V| \left(\frac{X-Y}{\sqrt{2}} \right)_{23}^{\otimes 2} \left(\frac{X+Y}{\sqrt{2}} \right)_{45}^{\otimes 2}, \\
M_7 &= X_1 X_2 X_3 (|HH\rangle_{45} \langle HH| + |VV\rangle_{45} \langle VV|), \\
M_8 &= (|HH\rangle_{23} \langle HH| + |VV\rangle_{23} \langle VV|) X_1 X_4 X_5, \\
M_9 &= (|HH\rangle_{23} \langle HH| + |VV\rangle_{23} \langle VV|) X_1 Y_4 Y_5, \\
M_{10} &= X_1 Y_2 Y_3 (|HH\rangle_{45} \langle HH| + |VV\rangle_{45} \langle VV|), \\
M_{11} &= Y_1 X_2 Y_3 (|HH\rangle_{45} \langle HH| - |VV\rangle_{45} \langle VV|), \\
M_{12} &= Y_1 Y_2 X_3 (|HH\rangle_{45} \langle HH| - |VV\rangle_{45} \langle VV|), \\
M_{13} &= (|HH\rangle_{23} \langle HH| - |VV\rangle_{23} \langle VV|) Y_1 Y_4 X_5, \\
M_{14} &= (|HH\rangle_{23} \langle HH| - |VV\rangle_{23} \langle VV|) Y_1 X_4 Y_5.
\end{aligned}$$

- [1] D. James, P.G. Kwiat, W. Munro, A. White, Phys. Rev. A 64, 052312 (2001).
- [2] M. Bourennane, *et al.*, Phys. Rev. Lett. 92, 087902 (2003).
- [3] O. Gühne, C.-Y. Lu, W.-B. Gao, J.-W. Pan, Phys. Rev. A (R) 76, 030305 (2007).
- [4] B.M. Terhal, Theor. Comput. Sci. 287, 313 (2002); O. Gühne *et al.*, Phys. Rev. A 66, 062305 (2002).